# LA-UR-11-11622

Approved for public release; distribution is unlimited.

| | |
|---|---|
| Title: | The Los Alamos Upper Ocean Model |
| Author(s): | Jones, Philip W<br>McWilliams, James<br>Zhao, Bin |
| Intended for: | Report |



Los Alamos
NATIONAL LABORATORY
—— EST.1943 ——

# The Los Alamos Upper Ocean Model

Bin Zhao, Phil Jones, and James McWilliams

July, 2011

**Abstract**

The upper-ocean model for short-term climate variability of Danabasoglu and McWilliams (2000) has been implemented in the NCAR Community Climate System Model ocean component POP. Major features of the model include the full dynamics for the upper ocean, a lower climatological tracer reservoir and a barotropic flow based on the total ocean depth. The resulting coupled system is capable of reaching an quasi-steady state within a few decades. Comparison with equilibrium solution of a conventional, full depth model shows that the upper-ocean model reproduces both the mean state quite well. Comparison with observations indicates that major model biases present in the full depth model also exist in the upper-ocean model solutions. The inter-model difference, however, is significantly smaller than the common model-observation discrepancies. The upper-ocean model also captures low frequency climate variability over most of the global ocean, except the mid-latitude North Atlantic where the deep ocean hydrographic changes dominate. This report demonstrates the upper-ocean model is an ideal tool for climate variability studies which require a well-defined equilibrated state and hypothesis testing for the active role of the deep ocean.

# 1 Introduction

Recent generation of coupled atmosphere-ocean general circulation models (AOGCMs), even without ad-hoc flux adjustment, are capable of producing a "stable" climate, i.e. no long term drift, under a given forcing (Covey et al. 2004). However, it typically takes a long "spin-up" time (often many hundreds to thousands of years) for climate models to do so (Covey et al. 2006). This time constraint is mainly set by long term adjustment of the abyssal ocean (Danabasoglu et al., 1996; Stouffer 2004; Danabasoglu 2004) to thermal and dynamic forcing from other components (e.g., the atmosphere and cryosphere). Even with the ever-increasing computer power, running coupled AOGCMs at standard resolutions for such a long time is still prihibitively expensive and only a few institutions can afford it. This significantly limits our ability to explore model parameter sensitivities or generate large sized ensembles for decadal climate predictions or future climate change projections (Collins et al. 2006).

On the other hand, most of the important climate interactions among the component systems occur over much shorter periods from weeks to decades (e.g., ENSO). If it is these phenomenan that are of interest, one may choose to circumvent the difficulty associated with the long term deep ocean adjustment, essentially decoupling the upper ocean from the abyssal. As a first order approximation, the slab ocean is being used to represent the upper ocean states in a climate system. The coupled atmosphere-slab ocean model can approach equilibrium much faster compared to coupled AOGCMs, thanks to the much smaller thermal inertia within the slab ocean. However, this one-dimentional representation of the upper ocean misses some important oceanic processes, in particular, dynamical heat transport, which could play important roles in modulating oceanic variabilities.

Although several idealized models have been proposed focusing on wind-driven upper-ocean dynamics on regional scales, Danabasoglu and McWilliams (2000; DM00 hereafter) presented an upper-ocean model (UOM) specifically for studying short-term climate variability on global scales. The underlying assump-

tion for UOM is that fluctuations in tracers (potential temperature and salinity, for example) tend to be confined above the pycnocline, suggesting short-term climate variability should be most intense down to this depth and shallower. They demonstrate that the greatest strength of the UOM lies in its much faster adjustment ($\sim$30 yrs) to equilibrium than a conventional, full depth ocean general circulation model (FDM). Any ambiguous trend in a non-equilibrium solution of a FDM will be eliminated in a UOM, given a suitable bottom boundary condition. The UOM does this in a dynamically consistent way.

DM00 implemented the UOM in an earlier version of the NCAR ocean model (NCOM), which lacks a few advanced characteristics of the current generation OGCMs. Furthermore, NCOM is no longer supported as the ocean component within NCAR coupled AOGCM system. Thus there is a need to bring the UOM onto the current climate research plateform. In this report, we document such an effort, describing the implementation of UOM in the Parallel Ocean Program (POP; Smith and Gent 2002) and evaluating its solution in a coupled context in the Community Climate System Model version 3 (CCSM3). In doing so, we identify the potential roles the abyssal ocean may play in driving surface climate. Yeager et al. (2006) documented a low resolution version of the CCSM3 (a T31 atmosphere and a $\times$3 ocean), which serves as the baseline simulation for our UOM configuration to compare. We expect the UOM to perform as well as the FDM POP in the upper ocean in CCSM3, but achieve this good performance with a much shorter integration time. More importantly, our UOM solution has no confusing ambiguity of the continuing, slow abyssal evolution present in the FDM.

The implementation of the UOM in POP along with the detailed configuration of CCSM3 is described in section 2. The coupled spin-up phase of the CCSM3 with the UOM POP is presented in section 3. The quality of the mean upper ocean simulation is assessed in section 4. The climate variability, in particular, the simulated ENSO, is analyzed in section 5. The final section discusses some sensitivity tests of the UOM and presents our conclusion.

4

# 2 Model Developement and Configuration

## 2.1 The UOM implementation in POP

For complete description of the design principles and model formulations of the UOM, see DM00. Here we briefly describe some technical aspects differing from its original incarnation. The primary difference is the model vertical coordinate. While DM00 implemented the UOM in a $\sigma$-coordinate model, its formulation fits more naturally in a geo-potential (z-) coordinate framework on which POP was built. Given that the depth of the bottom of the upper ocean (normally chosen just lying below the permanent pycnocline) is not uniform, fluxes through the UOM lower boundary at some locations come from both vertical and lateral directions. In DM00 fluxes appears coming in a vertical only direction because of the $\sigma$-coordinate. In practice, fluxes from both directions have to be assembled/interpolated to form the boundary condition. We avoid any complications associated with this extra process by employing the strategy below as to dealing with ocean states in the abyss. Additionally, there is no need to smooth the bottom topography in our model, as in a $\sigma$-coordinate model which otherwise has difficulty in computing pressure-gradient forces.

We choose to relax temperature and salinity fields at any grid point lying below the UOM bottom boundary to their climatologies which were obtained from a long time integration of a stand-alone FDM POP. We do the same to the horizontal velocity field but only for their baroclinic components. The total velocity can be computed by adding the prognostic barotropic component. Keeping these terms in deep ocean allows the UOM to reuse most of the POP code, e.g. advection schemes and subgrid scale parameterization, since they are readily available when needed to compute fluxes at bottom of the upper ocean. This is different from simply relaxing tracer fields to their climatology in deep ocean, which may distort barotropic dynamics, as pointed out in DM00. In our approach, the deep ocean still serves as a climatological reservior of tracers and baroclinic velocity with infinite capacity, consistent with the original design.

One must take great care when formulating momentum tendency terms for the barotropic solver, especially for those involving densities. As pointed out by DM00, any inconsistencies will cause spurious circulation to develope. In our experience, these errors can easily be identified by looking at barotropic steam functions. Still, we caution other practitioners who may implement the UOM in other ocean models that the pressure gradient force is the most error-prone term.

## 2.2  The CCSM3 Configuration

Collins et al. (2006a) gave an overview of the CCSM3 with its various components. In this study, we employ the low resolution version of the CCSM3. Yeager et al. (2006) documented some modifications specifically to this configuration to make it a viable alternative to higher resolution version of the CCSM3. The atmosphere component is the T31 version of the Community Atmosphere Model (CAM3: Collins et al. 2006b) with an equivalent grid spacing of approximately $3.75°$. The sea ice component is the Community Sea Ice Model (CSIM5: Briegleb et al. 2004) which contains the elastic-viscous-plastic (EVP) dynamic and thermodynamic core. The land surface model is the Community Land Model (CLM: Oleson et al. 2004) with grid identical to that of CAM3.

The ocean component is the $\times 3$ version POP with $100 \times 116$ grid points and 25 levels in vertical, thus has a nominal resolution of $3°$ in longitude and latitude. The resolution gets much higher in the Tropics and North Atlantic. CSIM5 uses this same grid as the POP. For the UOM POP, we follow DM00 to choose the bottom depth of the upper ocean. Roughly the UOM contains two thirds of the total number of grid points over the whole ocean volume. For the lower boundary conditions of the UOM, we first integrate a standalone FDM POP for 3000 years (for it to reach an equilibrium state, especially in the deep ocean) and then extract and construct 12 monthly climatological fields required. Where the UOM bottom coincides with the actual ocean bottom, it uses the same boundary conditions as in the FDM. No flux-adjustment is applied since

our model is able to maintain a stable climate.

Two simulations under the present-day (1990) atmospheric condition are performed, one with the FDM POP (hereafter CCSM3-FDM) and the other with the UOM POP (hereafter CCSM3-UOM). Both simulations starts from the same initial conditions. The ocean component is initialized with World Ocean Atlas 1998 climatology (Levitus et al. 1998) combined with the Polar Science Center Hydrographic Climatology (PHC) Arctic data (Steele et al. 2001). Both the UOM and FDM use the same set of physical parameters throughout the integration.

The primary goal of this study is to evaluate the equilibrium solution of the UOM as compared to the FDM. For this purpose, we use the difference between the two model solutions for most of our results. We do include observed datasets whenever they are available to highlight the model biases, most of which have also been addressed by Yeager et al. (2006), Large and Danabasoglu (2006), Deser et al. (2006), and Holland et al. (2006). The following observational datasets are used: sea level pressure (SLP) from the NCEP-NCAR reanalyses (Kalnay et al. 1996), sea surface temperature (SST) from the NOAA optimum interpolation sea surface temperature (OISST) analysis (Reynolds et al. 2002) during 1982-2004 and extended reconstructed sea surface temperatures (ERSSTv2; Smith and Reynolds 2004) during 1900-2004, and ice coverage from 1979-1999 Special Sensor Microwave Imager (SSMI) satellite data (Comiso 1999).

# 3    Approach to equilibrium

DM00 demonstrates that the UOM is capable of reproducing the FDM equilibrium solution within a matter of 2 to 3 decades in an ocean standalone run case. For comparison, Fig. 1 shows the global annual mean time series of the potential temperature ($\theta$) and salinity ($S$) for CCSM3-UOM and CCSM3-FDM. Both models are integrated for 500 yrs for secular trend (if any) and the full range of natural variabilities to realize. The CCSM3-UOM global mean $\theta$ appears to be

adjusting for a period of 40 yrs and then approaching a quasi-steady state. Contrary to DM00, CCSM3-UOM displays significant interannual to multi-decadal variabilities. The CCSM3-FDM also undergoes some adjustments during the first 200 yrs, and then follows a long term trend reflecting the abyssal ocean changes. Also shown in Fig. 1 is a 500-yr long time series which is taken from the CCSM3-FDM starting at yr 1501. This time series represents the quasi-equilibrium state the FDM reaches after a long time integration. The UOM achieves this state within only a few decades starting from a state of rest. In terms of temperature, our UOM implementation meets the original design goal.

There is a different time evolution for $S$. After an initial adjustment of about 25 yrs, $S$ deceases monotonically and reaches a steady state after about yr 400. Further analysis shows that both CCSM3-UOM and CCSM3-FDM have a small but relatively constant (throughout the integration) freshwater imbalance (expressed as a negative virtual salt flux in the model), which causes a freshening trend to develop. This trend is diminished until compensating salt transport, including advection and diffusion in/out of the UOM domain, balances the surface freshwater forcing. Apparently the corresponding time scale is O(100) yr even for the upper ocean. Another factor contributing to such a long time scale is that there is no local oceanic negative feedback on the surface freshwater flux, as opposed to the heat flux. Should the freshwater imbalance be absent, we expect $S$ in the UOM to reach a steady state with a similar time scale to $\theta$. Despite this caveat of the coupled model, we have not attempted to apply freshwater flux adjustment since the fast approaching to equilibrium of the UOM has been demonstrated by $\theta$.

It is difficult to determine an definite equilibration time scale as in DM00 because the equilibrium state in a coupled model consists of irregular oscillations over many time scales. An approximate estimate is 40-50 yrs for $\theta$. This may be a little bit longer than that in DM00, but still significantly shorter than that of the FDM. The average $\theta$ for CCSM3-UOM over the last 400 yr is 8.411 $°C$, compared to 8.402 $°C$ (averaged over yr 1501-2000) of the CCSM3-FDM at its equilibration time. Note also that the equilibrium values of $\theta$ for both CCSM3-

UOM and CCSM3-FDM are not far away from their initial values. For example, the difference is less than $0.1°C$ for CCSM3-UOM. This can be attributed to the careful initialization (the WOA/PHC in this case) of the model which Covey et al. (2006) propose as one of the contributing factors for boosted stability of the current generation of AOGCMs.

The transient behavior of the UOM over depth is depicted in Fig. 2. The departure of $\theta$ from the first year quickly stablised over all depths. This is in contrast to CCSM3-FDM (not shown) and other AOGCMs (e.g., Delworth et al., 2006) in which long term trend still exists after a few hundred years of integration, especially in subsurface ocean (between 400 and 1000 m). Consistent with surface freshwater imbalance, $S$ develops trends over all depths. However, they are clearly not uniform over depth, with shallower layers adjusting faster. The freshening trend is dominated by the top 100 meters, indicating the imbalanced freshwater (virtual salt) flux at the surface.

# 4    Mean state

## 4.1    Ocean

SST is probably the most important oceanic field at the ocean-atmosphere interface, determining the heat exchange between the two component systems. It also primarily varies on short climate time scales, which the UOM is designed to capture faithfully. Mean SST from CCSM3-UOM is shown in Fig. 3a, along with the differences from CCSM3-FDM (Fig. 3b) and observations (Fig. 3c). Clearly the UOM reproduces the SST pattern of the FDM over most of the globe, except in a few isolated regions of the northern North Atlantic, where deep convection frequently occurs and the differences reach more than $1\ °C$. SST also gets warmer by as much as $1.5\ °C$ in the northern part of the North Pacific. Both model solutions have biases compared to the observed data. Cold biases develop in the higher latitudes in both hemispheres, and warm biases appear along the eastern boundaries of the subtropical ocean basins (off the

coasts of south west Africa and north west South America). These dificiencies are also present in higher resolution CCSM3-FDM runs, presumably associated with some inherent problems of both the ocean and atmosphere model (Large and Danabasoglu, 2006). The former is particularly severe here due to the poorly simulated poleward heat transports and the latter not worse than those higher resolution runs (Yeager et al., 2006). Overall, the differences in SST between the UOM and FDM are much smaller than their differences from the observations. The same is true for the sea surface salinity (SSS; not shown).

To examine the mean ocean circulation, we look at the vertically integrated volume transport, or barotropic stream function (BSF) shown in Fig. 4a. The UOM formulation of the BSF is based on the full ocean depth, therefore can be directly compared to that of a FDM. In this formulation, the contribution of the deep ocean variables to the barotropic equation is simplified to include only their climatological components. The resulting transport is typical of ocean GCMs at similar resolutions (DM00). In particular, the maximum transports in the subtropical gyres of the North Pacific and North Atlantic are less than 50 and 40 Sv, respectively, while both exceed these values in the high resolution version (T85x1) of the CCSM3 (Large and Danabasoglu, 2006). The subpolar gyre transport of the North Atlantic is over 40 Sv, comparable to T85x1. The South Atlantic subtropical gyre is weaker than T85x1, but closer to observed values (Large and Danabasoglu, 2006). The BSF difference between CCSM3 -UOM and CCSM3-FDM (Fig. 4b) is generally small, except in the Antarctic Circumpolar Current (ACC) region where > 4 Sv difference is observed. The ACC transport exhibits some long time scale fluctuations (not shown; see Yeager et al., 2006 and Delworth et al., 2006) so the difference shown here may depend on the time period over which the mean is taken. Regardless, the close correspondence suggests that the slow-varying part of the deep ocean states is not important to mean barotropic transport.

It is equally important for the UOM to have a realistic meridional over-turning circulation (MOC) with implied poleward heat and salt transport to maintain a stable climate. The MOC in the upper ocean can be determined

10

freely by the UOM without any constraint from the bottom boundary conditions. The global mean meridional overturning streamfunction, obtained only with the Eulerian mean velocity, is shown in Fig. 5a. The downwelling concentrated between 30 and 60 $^{\circ}N$ is mainly associated with deep water formation in the North Atlantic, which is almost as strong as that of CCSM3-FDM (Fig. 5b). Both overturnings are less vigorous than the high resolution models (e.g., T85x1). In the Southern Hemisphere, the Deacon cell (its top part) is especially strong (reaching over 40 Sv), due to exclusion of the eddy-induced transports. Over both sides of the equator, there are two strong shallow overturnings above 300m caused by the Ekman transport. The difference between CCSM3-UOM and CCSM3-FDM is smaller than 1 Sv almost everywhere. The close resemblance of the overturning circulations again suggests that the UOM is dynamically consistent with the FDM.

The mean zonal velocity at the Equatorial Pacific is presented in Fig. 6. The structure of the zonal flow is almost indistinguishable between CCSM3-UOM and CCSM3-FDM. They both have a weaker Equatorial Under Current (EUC) core ($< 90 \ cm \ s^{-1}$) than observations ($> 100 \ cm \ s^{-1}$; Yeager et al., 2006). The EUC core is also flattened in both models, instead of tilting eastward as in observations. The successful simulation of the tropical surface and subsurface circulations by the UOM is critical should it be used to study such climate variabilities as ENSO.

## 4.2   Sea ice

Although the UOM is anticipated to be primarily used for tropical problems, the sea ice distributions in polar regions are still important diagnostics under coupled context because of their modulating role of the climate change and variability, thus merits our evaluation. Generally CCSM3-UOM produces a slightly less extensive sea ice content in the Northern Hemisphere than CCSM3-FDM (Fig. 7, top), mainly in the Barents Sea and its southern border, consistent with the warmer SST (Fig. 3b) there. The difference, however, is significantly

11

smaller than the model-observation difference (see the bold line representing the observed climatological location of 10% ice coverage from SSMI). The model bias is particularly big in the Labrador Sea, the Sea of Okhotsk and the Barents Sea where the ice edge extends too far south. Yeager et al. (2006) attributed this latter bias to a cold bias ($>$ 12 $^\circ C$) of the surface air temperature. This in turn may results from an insufficient oceanic heat transport, which is true for both models at low resolution. On the contrary, the higher resolution configuration (T42x1) produces less sea ice extent than observations in the Barents Sea (Holland et al., 2006).

The Southern Hemisphere sea ice distribution is also characterized by the overall too extensive ice coverage as compared to observations (Fig. 7, bottom), especially in the Atlantic sector of the Southern Ocean. Despite these biases, the two models agree with each other very well.

In summary, the sea ice simulation in CCSM3-UOM is quantitatively not much different from CCSM3-FDM. Same biases are present in both models. This is again expected given that sea ice is strongly affected by the oceanic heat transports and the UOM more or less resembles the FDM in this respect (section 4).

# 5   Climate variability

Climate variabilities over many time scales are generated by either the external climatic forcing, or the coupled climate model itself, or both. By construction, the UOM bottom boundary conditions only contain annual cycles of the tracer and baroclinic velocity fields. Therefore, one may question whether the upper ocean variability may be altered due to coupling to a non-interactive deep ocean. As demonstrated below, major climate modes in the UOM are comparable to those in the FDM, suggesting that the relevant mechanisms are fully captured by the UOM. Note that our coupled setup allows more modes of variability to develope, while such modes may be supressed in DM00's ocean-only runs. We stress that for those modes on much longer-time scales (multi-decadal and

beyond), primarily involving the MOC changes, the UOM might not be an ideal tool because of the invariant deep ocean state.

## 5.1   Global pattern

From a global perspective, we examine the standard deviation of annual mean SST anomaly (Fig. 8). In addition to comparison with the FDM, we also include the result from a coupled slab ocean model (SOM). The difference between the UOM/FDM and SOM reveals the role of the oceanic processes in producing climate variations, while the difference between the UOM and FDM shows the effect of deep ocean processes. In general, both GCMs show major climate signals in the tropical Pacific (ENSO), middle to high latitudes in the Northern Hemisphere, and the Southern Ocean. The SOM, however, misses almost all of these variabilities, notably, ENSO and those along the subtropic-subpolar gyre boundary. The results here are in general agreement with previous studies, e.g., Manabe and Stouffer (1996) and Hall and Manabe (1997). In SOM, the SST variability over the open ocean simply follows the local linear stochastic theory (Hasselmann 1976). In both GCMs, however, only a portion of the global ocean (far away from strong currents) bears this as a primary mechanism.

At depth, the UOM also reproduced the basic pattern of upper ocean FDM variabilibty quite well (Fig. 9). The skill for tropical and subtropical/subpolar subsurface signals is particularly good. At very high latitudes, e.g., north of $60^o N$, the UOM seems underestimating variabilities below 200m. As mentioned previously, this occurs where the upper ocean approximation breaks down. Regardless, here our result suggests that the mechanisms governing the upper ocean anomalies, as explained by Doney et al. (2007) in an ocean model hindcast, are adequately preserved in the UOM. We also tested sensitivity to UOM bottom topography by making it uniform at 1280m depth everywhere. There is no appreciable difference (Fig. 9c), though the equilibration time scale is somewhat longer (not shown) due to small diffusivities below the pycnocline in the Tropics.

Although the UOM agrees well with the FDM over most of the global ocean, an area with eye-catching difference is in the vicinity of east coast of the U.S. where the model Gulf Stream starts to detach from the continental coast. Here the FDM has twice as big SST variance as in the UOM, indicative of some contribution from the deep ocean. SST anomalies in this region could be generated by north-south shifting of the subtropical-subpolar gyre boundary. Danabasoglu (2008) shows such an effect, induced by surface wind stress curl (WSC), on SST anomalies in a high resolution version CCSM3. Nevertheless, it has been well known that the gyre transport is not only determined by WSC, but also by the potential density structure in the deep ocean through the joint effect of baroclinicity and relief (JEBAR; Sarkisyan and Ivanov, 1971; Greatbatch et al., 1991; Meyers and Weaver, 1996; Born et al. 2009). By design, the UOM omits changes (mostly originating from high latitudes where deep water forms) in the deeper part of the JEBAR term, hence a potential forcing mechanism is mssing. In the UOM, this happens within a small region near the western boundary in the mid-latitude North Atlantic.

To test the above hypothesis, we follow Danabasoglu (2008) and compute a gyre boundary index (GBI). We use latitudinal changes of the zero isocontour of the barotropic streamfunction (BSF) along $60°W$. Fig. 10a and 11a show the power spectra of the time series of GBI for FDM and UOM, respectively. The FDM has a significant peak (at 95% level) at a period of about 33 years and most variance in lower frequencies, whereas the UOM, having a much lower variance, peaks at a period less than 10 years. Consistent with power spectra of the GBI, the local SST exhibits much stronger variability near low frequency in the FDM (Fig. 10b) than in the UOM (Fig. 11b). This strong low-frequecy shifting of the gyre boundary in the FDM results from the deep ocean density changes (associated with transport by the deep western boundary currents), not the WSC, as confirmed by the the regression of the latter onto the GBI (Fig. 10f). In the UOM, the WSC seems able to explain a major portion of the variance (Fig. 11f) since (deep) part of the dominant JEBAR term is missing. Based on GBI, we construct composites corresponding to difference between

14

the states when gyre boundary at its most northern (NORTH) and southern (SOUTH) positions. NORTH (SOUTH) is defined as those years when latitude difference from the mean exceeding one standard deviation. The composite SSTs (Fig. 10e and 11e) clearly show that warming due to gyre shift is much stronger in the FDM than in the UOM, consistent with the rms map in Fig. 8. The BSF composites (Fig. 10d and 11d) also show distinct structures with the FDM having positive maximum near western boundaries and the UOM in the mid-basin where the WSC is dominating. Finally, the potential density (averaged over the abyssal ocean domain) composite in the FDM (Fig. 10c) indicates that the deep ocean south of the Grand Banks undergoes significant changes, which contribute to the gyre transport fluctuations.

We note that this UOM-FDM difference can vary from model to model, or from one resolution to another. The exact locations highly depend on the actual variations in the local deep ocean potential density. Typically in a coarse resolution configuration, like the one in this study, the deep western boundary currents are weak, and the associated density changes are small. We expect the JEBAR effect to be more pronounced in a model with more refined topographic features and less diffusive circulations.

## 5.2 ENSO

We next focus on ENSO since it has a global impact and realistically capturing its variability still represents a major challenge to the current generations of AOGCMs (Deser et al. 2006; Wittenberg et al. 2006). For the T31x3 CCSM3 used in this study, the hope is only that the simulation is not significantly degraded compared to the two higher resolutions (Yeager et al. 2006). We utilize a 500-yr time series of monthly SST anomalies in the Niño-3.4 region (101-600 for CCSM3-UOM and 1501-2000 for CCSM3-FDM) to analyze ENSO variability. Fig. 12 shows the Niño-3.4 SST index for observed and two models. Here only a 105-yr segment (1900-2004) corresponding to ERSSTv2 is shown and the same length of the model series are taken. A first impression is that the

15

two models generate more frequent and regular viariabilities than observations. Among the three time series, CCSM3-UOM has the smallest amplitude of variability. Indeed, the std. of CCSM3-UOM over the whole 500-yr is 0.83 $^\circ C$, compared to 0.85 $^\circ C$ for both CCSM3-FDM and ERSSTv2. By this measure, the FDM seems outperforming the UOM. Analysis of the HADISST by Deser et al. (2006), however, gives a std. of 0.75 $^\circ C$ over 1900-2003 and two higher resolution configurations overestimate it. It is clear that whether CCSM3-UOM or CCSM3-FDM is more close to observations depends on which data product is used, and both models have a Niño-3.4 variability amplitude well within the range observational uncertainties allow. One definite fact nevertheless is that CCSM3-UOM has a slightly weaker ENSO variability than CCSM3-FDM. A possible cause may be related to the mean state SST in the central equatorial Pacific. There CCSM3-UOM is slightly warmer than CCSM3-FDM (the whole area north of the Equator and $150^\circ W - 120^\circ W$ south of the Equator; Fig. 3b), which, along with other unknown potential factors (requires further analysis), could help reduce the SST variability.

Fig. 13 shows the power spectra of the Niño-3.4 SST index for models and observations. The ERSSTv2 has broad spectral peaks spanning over periods 3-8 yrs. Both models have a more narrow-banded spectra, consistent with their regularity shown in Fig. 12, with dominant period (2.49 yrs) for CCSM3-UOM slightly longer than that (2.19 yrs) for CCSM3-FDM. As indicated above, the amplitudes of oscillations for CCSM3-UOM are smaller than both CCSM3-FDM and observations. Also note that increasing model resolutions broadens the spectral peak, as shown in Deser et al. (2006; see Fig. 13 and their Fig. 3). Additional wavelet analysis (not shown) reveals that CCSM3-FDM has its peak power shifted to a period between 3 and 6 yr during the model yr 1560-1620, while similar power shifting is not observed during any interval in CCSM3-UOM.

Another well observed ENSO variability feature is its phase locking to the annual cycle, with weakest variability in May and strongest variability in December (see Fig. 14, red line). This feature is qualitatively reproduced by both models (Fig. 14, blue and green lines), albeit with some differences. Both mod-

els exhibit somewhat stronger variabilities through July to September, besides the peak in December. So instead of an annual locking, both models tend to have a semiannual locking, as also noted by Wittenberg et al. (2006) in GFDL's CM2 model. In January and February, when observations still show some peak events, both models give a variance minimum. The phase relationship is the same in both models, with CCSM3-UOM having a weakly reduced amplitude for almost all calendar months (also see above).

Fig. 15 shows the spatial patterns of ENSO-associated changes in precipitation and zonal surface WS ($\tau_x$). Accompanying the warm events, there is an equatorial precipitation peak centered around $180°$ in observations, with dry conditions developing to the south and wet conditions emerging in a small area to the north. In the eastern equatorial Pacific, the observed rainfall also increases slightly, mostly concentrated to the north of the equator. Both models more or less capture the wet center, while the rainfall anomalies are too symmetric about the equator in the central Pacific, probably a symptom of the double ITCZ. At the same time, the zonal WS response to Niño-3.4 SST anomalies are westerly anomalies over the central equatorial Pacific ($180°W - 150°W$), which are present in both observations and two models, but the model responses are too weak. The meridional extent in two models is also too narrow, and the structure is too zonal compared to observations. The former has been attributed to the shorter period of the simulated ENSO in CCSM3 (Deser et al. 2006). Despite these differences between models and observations (also see their presence in CM2 model in Wittenberg et al. (2006)), the distinction between two models are very minor, suggesting that the existing model biases in FDM are directly translated to the UOM and no other systematic errors appear due to the UOM formulation.

Overall, ENSO variability is reasonably well simulated by the UOM with only moderate differences from the FDM. As mentioned above, the abyssal tracer reservoir here is a good approximation which seems not affecting fields evolution in the surface ocean. Again, all relevant dynamic and thermodynamic processes with associated feedbacks are captured within the UOM domain.

17

## 5.3  Annular mode

As a final analysis, we look at the simulated Arctic Oscillation (AO) and Antarctic Oscillation (AAO). Fig. 16 shows the first empirical orthogonal function (EOF) of mean December-February sea level pressure (SLP) in the Northern Hemisphere and monthly SLP anomalies (by subtracting the seasonal cycle) in the Southern Hemisphere. For comparison, NCEP-NCAR reanalysis over 1948-2006 is also shown in Fig. 16. The AO mode in two models looks very similar to each other, and both show a tripolar pattern. The two centers-of-action in the North Atlantic appear to have westward shifted positions and stronger amplitudes, as compared to the NCEP data. The third center is absent in observations. The AAO modes in two models are almost identical, and they both look much stronger than observations. For both the AO and AAO, the first EOF of the models explains a bigger chunk of variance than that of the NCEP. Similar to many other diagnostics above, difference between the UOM and FDM is overwhelmed by the their discrepancy from observations.

# 6  Discussion and conclusions

We have described an UOM implementation in POP model and tested it in a coupled context with CCSM3. We have extended the work of DM00 in two major ways: 1) we implemented the UOM in POP and coupled it within the CCSM3, both of which greatly expanded its scope of usability; 2) we carried out multi-century simulations with it and analyzed climate variability in more detail. Simulations under present-day conditions show that the coupled system with the UOM approaches a steady state within about a few decades, effectively achieving the original design aim. Furthermore, the UOM produces a mean state and variabilities almost the same as the FDM in its quasi-equilibrium state, except for a few localized regions. Major differences include: warmer SST in middle to high latitudes and in the tropical Pacific, different ACC barotropic transport, slightly less extensive sea ice coverage in the Northern Hemisphere, weaker mid-

18

latitude SST variability near western boundary currents in the North Atlantic and ENSO variability.

Ideally the UOM bottom is chosen to lie below the climatological pycnocline such that most of the short-term tracer variations are confined within the upper ocean domain. In this study, we follow DM00 and only approximately choose it this way. We note that in the real ocean the pycnocline may exceeds the model bottom depth. At high latitudes, large diffusivities associated with intermittent deep convection (possibly induced by the freezing of sea ice and brine formation) may propagate tracer anomalies through the bottom into the abyssal ocean. Since the UOM treats the abyssal ocean as a climatological reservoir, flux inconsistencies are generated at the lower interface in the UOM formulation, although they may be small (DM00; see Fig. 17d). This can be quantified by looking at the heat exchange at the bottom, as shown in Fig. 17c. We can see the majority of such events occur in the northern North Atlantic (the Labarador Sea and Greenland Sea) and throughout the Southern Ocean, where the upper ocean is cooled by convective mixing. Everywhere else the flux is small, indicating that the upper ocean approximation is accurate. There are also some vertical advective heat fluxes through the lower boundary (Fig. 17a), which shows a somewhat complex pattern. These fluxes are compensating with each other, however, and their average effect on the upper ocean is only marginal (less than 1 $Wm^{-2}$), whereas the diffusive fluxes amount to 5 $Wm^{-2}$.

Model physics and parameter choices may affect the upper ocean equilibration time scales. We have run a CCSM3-UOM case (denoted hereafter CCSM3-UOMK) with a larger and depth independent vertical diffusion coefficient (the same value as in DM00). Relative to CCSM3-UOM, CCSM3-UOMK has enhanced diffusion near surface. Change in diffusion coefficient, however, does not affect the adjustment time scale for temperature. The salinity equilibration time seems to be shortened. Due to the freshwater imbalance, this may not reflect the true time scales in the upper ocean anyway. For both temperature and salinity, there is large deviations of equilibrium values from CCSM3-FDM. As to model physics, we have run another sensitivity test case for CCSM3-UOM with

a 3rd-order upwind tracer advection scheme replacing the centered difference scheme. Overall this physics change has no impact on either equilibration times or values for temperature, and only slightly changes salinity. It does induce some changes in the mean state and variability pattern, e.g., more extensive sea ice coverage in the Northern Hemisphere, and weaker ENSO variability. Considering that the higher resolution configurations of CCSM3 have similar parameters and the same model physics, we anticipate they also have similar upper ocean equilibration time scales to that of CCSM3-UOM.

Our companion UOM/FDM simulations suggest a high to middle latitudes and deep to surface link, in which hydrographic changes in the deep water formation (DFW) regions have a profound impact on SST along the gyre boundaries. The mechanism involves the deep transport of dense waters from higher latitudes and its interaction with bottom topography (JEBAR), which has been invoked to explain the path and separation of the Gulf Stream and gyre circulation changes (Greatbatch et al. 1991; Meyers et al. 1996; Zhang and Vallis 2007; Born et al. 2009), but not for the low frequency climate variability. Our result further emphasizes the key role of density gradient below the permanent thermocline, as opposed to Meyers et al. (1996) who argued for the importance of the density fields in the upper water column. Note that this differs from those proposed in previous studies (e.g., Grötzner et al. 1998; Eden and Willebrand 2001) which rely on a baroclinic adjustment of the gyres to WSC variations. If the mechanism indeed is working in the real climate system, it merits more extensive monitoring of the overflows from the Arctic Ocean and Nordic Seas and convection in the Labrador Sea, and their faithful representation in ocean GCMs (Bailey et al. 2005; Born et al. 2009).

We believe that the current CCSM-UOM framework represents an ideal tool for hypothesis testings about the roles of deep ocean in climate change and variability, which have been far less appreciated because of scarce existent observations. We have demonstrated that it can be applied to interprete the effect of JEBAR on low frequency oceanic surface variabilities. Another possible venue for this model is related to the recent effort in Decdal Climate Prediction

(DCP) project. For DCP, the intial ocean state is critical for any meaningful forcast skills (Pohlmann et al. 2009). However, it is not clear whether accurate initialization of the abyssal ocean (below 2000m) states is mandetory. Such a problem could be tackled by running the UOM with several different sets of bottom boundary conditions and analyzing the difference in the resultant climate variabilities. Our experience with JEBAR suggests the answer might be yes.

# References

[1] Bailey, D. A., P. B. Rhines, and S. Häkkinen, 2005: Formation and pathways of North Atlantic Deep Water in a coupled ice-ocean model of the Arctic-North Atlantic Oceans. *Clim. Dyn.*, 25, 497-516.

[2] Born, A., A. Levermann, and J. Mignot, 2009: Sensitivity of the Atlantic Ocean circulation to a hydraulic overflow parameterisation in a coarse resolution model: Response of the subpolar gyre. *Ocean Modelling*, 27, 130-142.

[3] Briegleb, B., C. Bitz, E. Hunke, W. Lipscomb, M. Holland, J. Schramm, and R. Moritz, 2004: Scientific description of the sea ice component in the Community Climate System Model, version 3. Tech. Rep. TN-463 STR, NCAR 70 pp. [Available from NCAR, P.O. Box 3000, Boulder, CO 80307.]

[4] Collins, W. D., C. M. Bitz, M. L. Blackmon, G. B. Bonan, C. S. Bretherton, J. A. Carton, P. Chang, S. C. Doney, J. J. Hack, T. B. Henderson, J. T. Kiehl, W. G. Large, D. S. McKenna, B. D. Santer, and R. D. Smith, 2006: The Community Climate System Model Version 3 (CCSM3). *J. Clim.*, 19, 2122-2143.

[5] Collins, W. D., and Coauthors, 2006: The Formulation and Atmospheric Simulation of the Community Atmosphere Model Version 3 (CAM3). *J. Clim.*, 19, 21442161.

[6] Comiso, J., 1999: Bootstrap sea ice concentrations for NIMBUS-7 SMMR and DMSP SSM/I. National Snow and Ice Data Center.

[7] Covey, C., K. M. AchutaRao, U. Cubasch, P. Jones, S. J. Lambert, M. E. Mann, T. J. Phillips, and K. E. Taylor, 2003: An overview of results from the Coupled Model Intercomparison Project. *Global Planet. Change*, Volume 37, Issues 1-2, Evaluation, Intercomparison and Application of Global Climate Models, 10 June 2003, Pages 103-133, ISSN 0921-8181, DOI: 10.1016/S0921-8181(02)00193-5.

[8] Danabasoglu, G., 2004: A comparison of global ocean general circulation model solutions with synchronous and accelerated integration methods. *Ocean Modelling*, 7, 323-341.

[9] Danabasoglu, G., 2008: On Multidecadal Variability of the Atlantic Meridional Overturning Circulation in the Community Climate System Model Version 3. *J. Clim.*, 21, 55245544.

[10] Danabasoglu, G., and J. C. McWilliams, 2000: An upper-ocean model for short-term climate variability. *J. Clim.*, 13, 3380-3411.

[11] Danabasoglu, G., J. C. McWilliams, and W. G. Large, 1996: Approach to equilibrium in accelerated global oceanic models. *J. Clim.* 9, 1092-1110.

[12] Deser, C., A. Capotondi, R. Saravanan, A. S. Phillips, 2006: Tropical Pacific and Atlantic Climate Variability in CCSM3. *J. Clim.*, 19, 24512481.

[13] Delworth, T. L., and Coauthors, 2006: GFDL's CM2 Global Coupled Climate Models. Part I: Formulation and Simulation Characteristics. *J. Clim.*, 19, 643674.

[14] Doney, S. C., S. Yeager, G. Danabasoglu, W. G. Large, and J. C. McWilliams, 2007: Mechanisms Governing Interannual Variability of Upper-Ocean Temperature in a Global Ocean Hindcast Simulation. *J. Phys. Oceanogr.*, 37, 1918-1938.

[15] Eden, C., and J. Willebrand, 2001: Mechanism of Interannual to Decadal Variability of the North Atlantic Circulation. *J. Clim.*, 14, 2266-2280.

[16] Greatbatch, R., A. Fanning, A. Goulding, and S. Levitus, 1991: A Diagnosis of Interpentadal Circulation Changes in the North Atlantic. *J. Geophys. Res.*, 96(C12), 22009-22023.

[17] Grötzner, A., M. Latif, and T. P. Barnett, 1998: A Decadal Climate Cycle in the North Atlantic Ocean as Simulated by the ECHO Coupled GCM. *J. Clim.*, 11, 831-847.

[18] Hall A., and S. Manabe, 1997: Can Local, Linear Stochastic Theory Explain Sea Surface Temperature and Salinity Variability? *Clim. Dyn.*, 13, 167-180.

[19] Hasselmann, K., 1976: Stochastic climate models. Part 1. Theory *Tellus* 8, 392-400

[20] Holland, M. M., C. M. Bitz, E. C. Hunke, W. H. Lipscomb, and J. L. Schramm, 2006: Influence of the sea ice thickness distribution on polar climate in CCSM3. *J. Clim.*, 19, 2398-2414.

[21] Kalnay, E., and Coauthors, 1996: The NCEP/NCAR 40-Year Reanalysis Project. *Bull. Amer. Meteor. Soc.*, 77, 437471.

[22] Large, W. G., and G. Danabasoglu, 2006: Attribution and impacts of upper-ocean biases in CCSM3. *J. Clim.*, 19, 2325-2346.

[23] Levitus, S., T. Boyer, M. Conkright, D. Johnson, T. OBrien, J. Antonov, C. Stephens, and R. Gelfeld, 1998: Introduction. Vol. 1, World Ocean Database 1998, NOAA Atlas NESDIS 18, 346 pp.

[24] Manabe, S., and R. J. Stouffer, 1996: Low-Frequency Variability of Surface Air Temperature in a 1000-Year Integration of a Coupled Atmosphere-Ocean-Land Surface Model. *J. Clim.*, 9, 376-393.

[25] Myers, Paul G., Augustus F. Fanning, Andrew J. Weaver, 1996: JEBAR, Bottom Pressure Torque, and Gulf Stream Separation. *J. Phys. Oceanogr.*, 26, 671683.

[26] Oleson, K. W., and Coauthors, 2004: Technical Description of the Community Land Model (CLM). NCAR Tech. Note NCAR/TN-461+STR, 173 pp.

[27] Pohlmann, H., J. H. Jungclaus, A. Khl, D. Stammer, and J. Marotzke, 2009: Initializing Decadal Climate Predictions with the GECCO Oceanic Synthesis: Effects on the North Atlantic. *J. Climate*, 22, 3926-3938.

[28] Reynolds, R. W., N. A. Rayner, T. M. Smith, D. C. Stokes, and W. Wang, 2002: An Improved In Situ and Satellite SST Analysis for Climate. *J. Clim.*, 15, 1609-1625.

[29] Sarkisyan, A. S., and V. F. Ivanov, 1971: Joint effect of baroclinicity and bottom relief as an important factor in the dynamics of sea currents. *Izv. Acad. Sci., USSR Atmos. Oceanic Phys.* (Engl. transl.), 7, 173-178.

[30] Smith, R., and P. Gent, 2002: Reference manual for the Parallel Ocean Program (POP). Tech. Rep. LAUR-02-2484, Los Alamos National Laboratory, Los Alamos, New Mexico.

[31] Smith, T. M., and R. W. Reynolds, 2004: Improved Extended Reconstruction of SST (1854-1997). *J. Clim.*, 17, 24662477.

[32] Steele, M., R. Morley, and W. Ermold, 2001: PHC: A global ocean hydrography with a high-quality Arctic Ocean. *J. Clim.*, 14, 20792087.

[33] Stouffer, R. J., 2004: Time Scales of Climate Response. *J. Clim.*, 17, 209-217.

[34] Wittenberg, A. T., A. Rosati, N.-C. Lau, and J. J. Ploshay, 2006: GFDL's CM2 global coupled climate models. Part III: Tropical Pacific climate and ENSO. *J. Clim.*, 19, 698-722.

[35] Yeager, S. G., C. A. Shields, W. G. Large, and J. J. Hack, 2006: The Low-Resolution CCSM3. *J. Clim.*, 19, 2545-2566.

[36] Zhang, R., and G. K. Vallis, 2007: The Role of Bottom Vortex Stretching on the Path of the North Atlantic Western Boundary Current and on the Northern Recirculation Gyre. *J. Phys. Oceanogr.*, 37, 2053-2080.
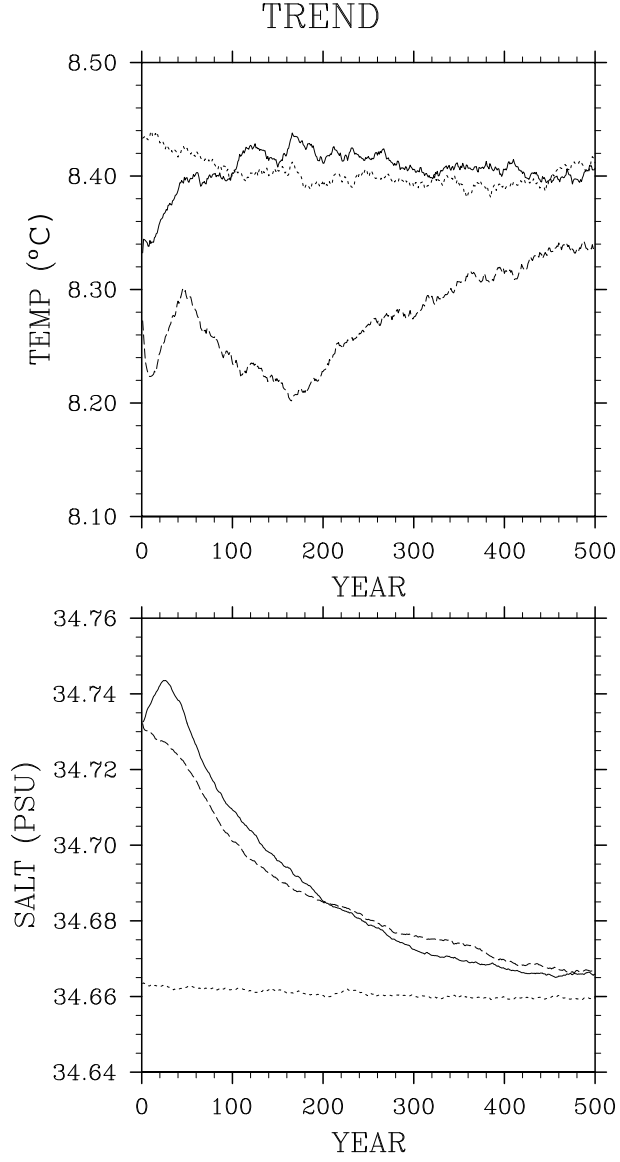
Fig. 1: Time series of the global and annual mean $\theta$ ($^\circ C$) and S ($PSU$) for cases
CCSM3-UOM (solid line), CCSM3-FDM (long dashed line), and CCSM3-FDM
at its equilibrated state (short dashed line; see text).
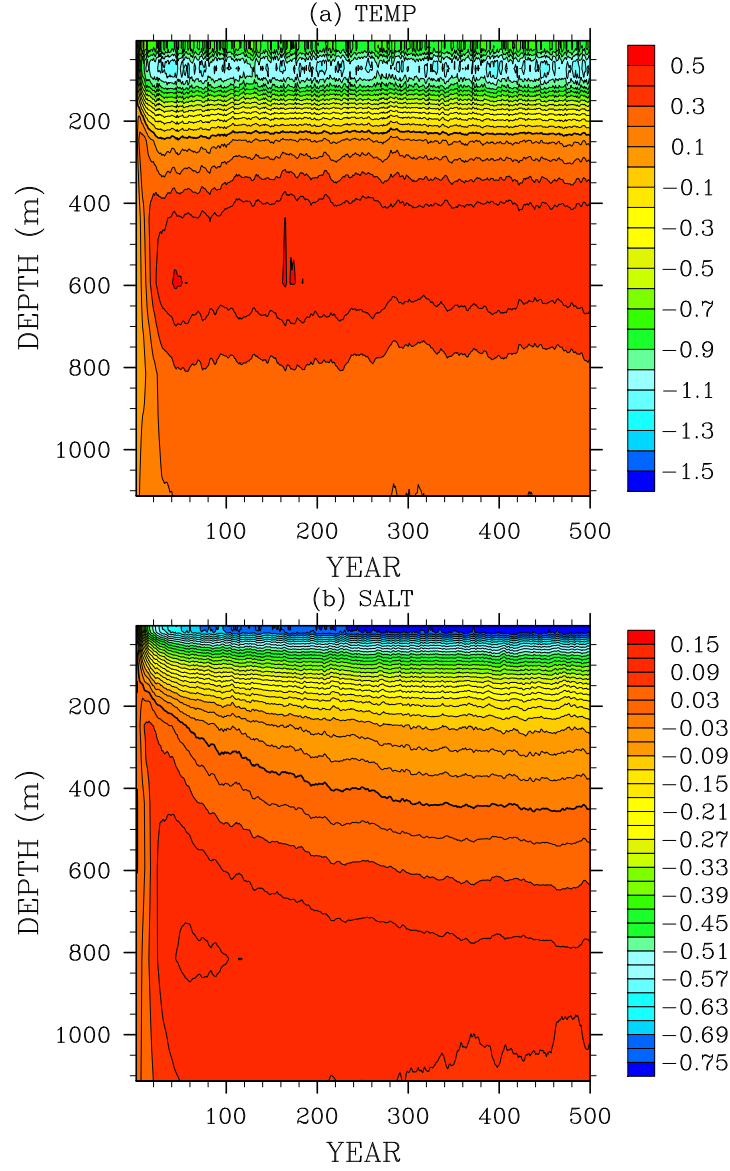
Fig. 2: Deviation of the globally and annually averaged (a) $\theta$ ($^{\circ}C$) and (b) S ($PSU$) from the first year for CCSM3-UOM as a function of depth. Zero-contours are thickened.

27
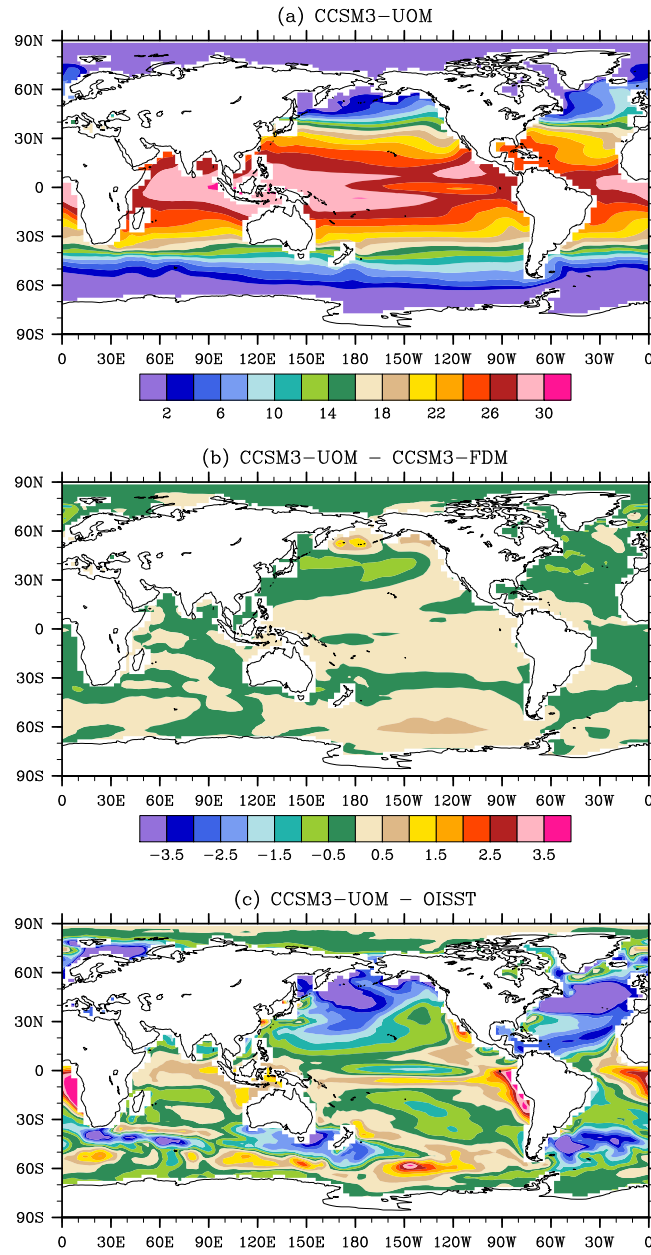
Fig. 3: Time-mean SST (in $^\circ C$). (a) CCSM3-UOM, (b) CCSM3-UOM difference from CCSM3-FDM, and (c) CCSM3-UOM difference from observations. CCSM3-FDM mean is over yr 1980-1999.
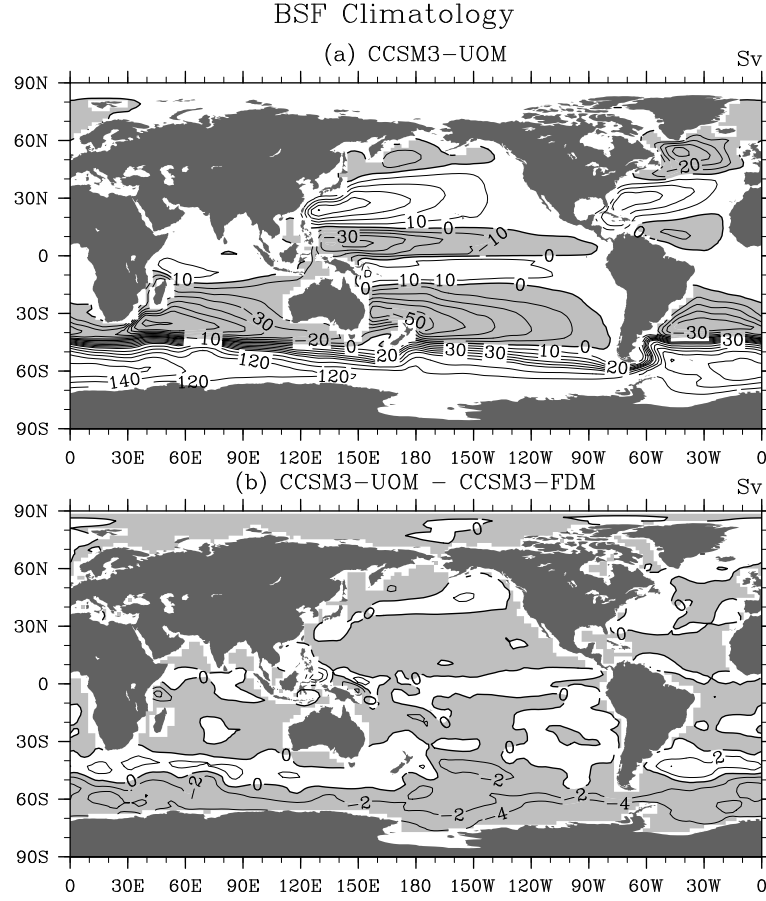
Fig. 4: Time-mean BSF. (a) CCSM3-UOM, the contour intervals are 10 and 20 Sv for transports smaller and greater than 80 Sv, respectively. Positive and negative (shaded) contours indicate clockwise and counterclockwise circulations. (b) CCSM3-UOM difference from CCSM3-FDM, the contour interval is 2 Sv, and the negative regions are shaded.
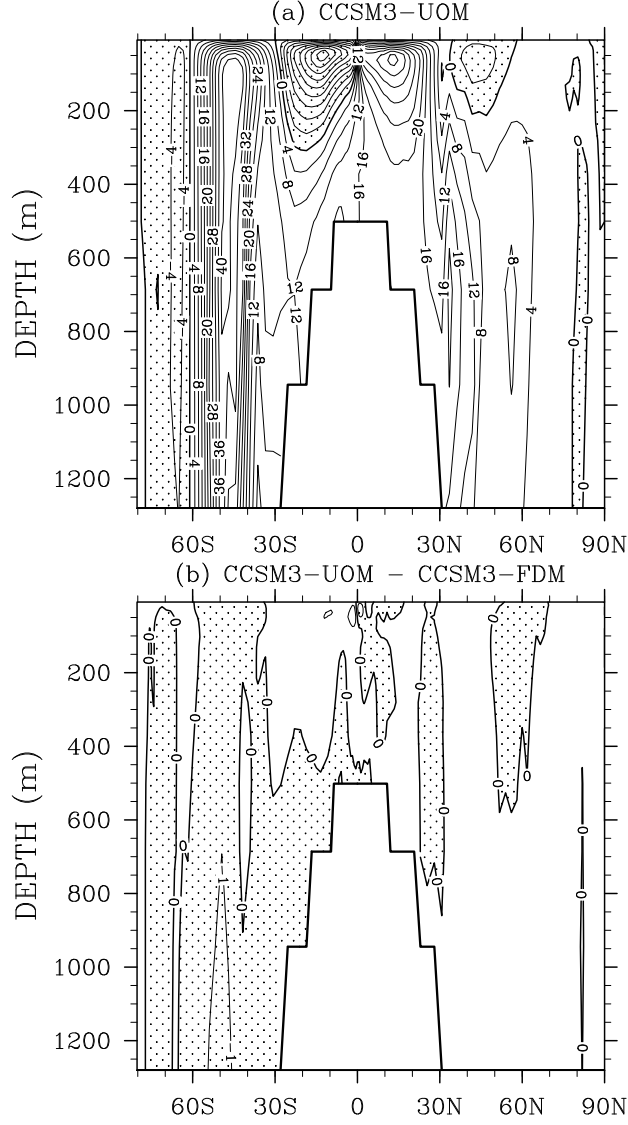
Fig. 5: Time-mean, zonally integrated meridional overturning stream function obtained with the Eulerian mean velocity only. (a) CCSM3-UOM, the contour interval is 4 Sv, and positive and negative (shaded) contours indicate clockwise and counterclockwise circulations, respectively. (b) CCSM3-UOM difference from CCSM3-FDM, the contour interval is 1 Sv, and the negative regions are shaded. The thickened step-like curve represents the bottom of the upper ocean domain.

30

# U at Equator

## (a) CCSM3−UOM
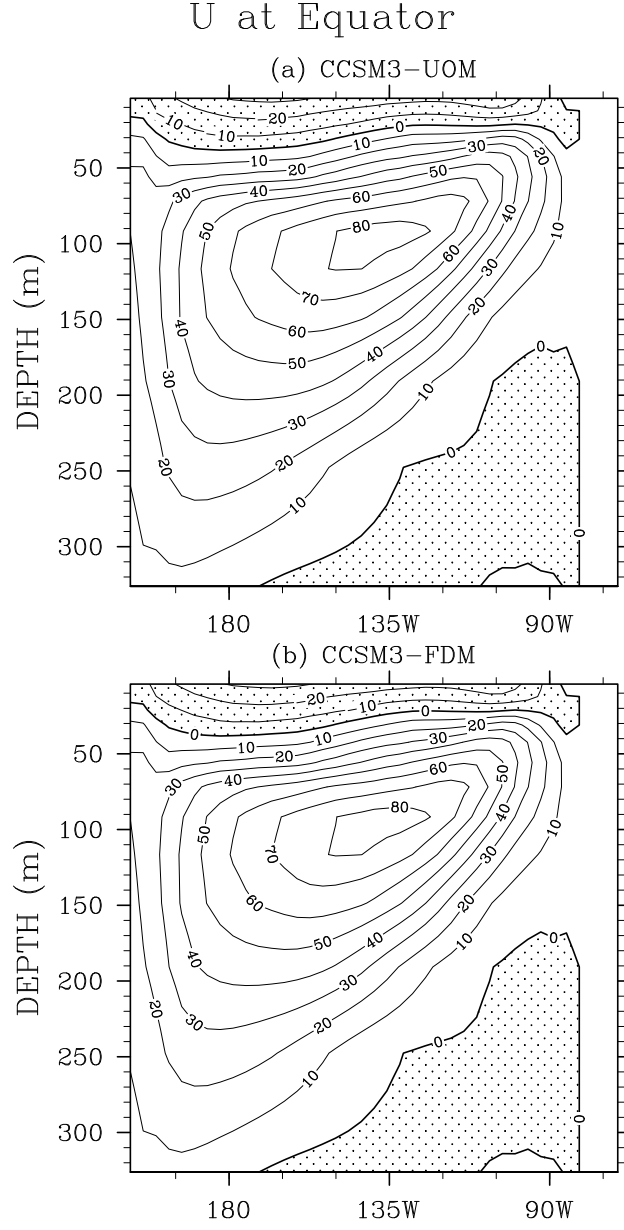


## (b) CCSM3−FDM



Fig. 6: Time-mean Pacific zonal velocity at the equator from (a) CCSM3-UOM and (b) CCSM3-FDM. The contour interval is 10 cm/s, and the westward flow regions are shaded.
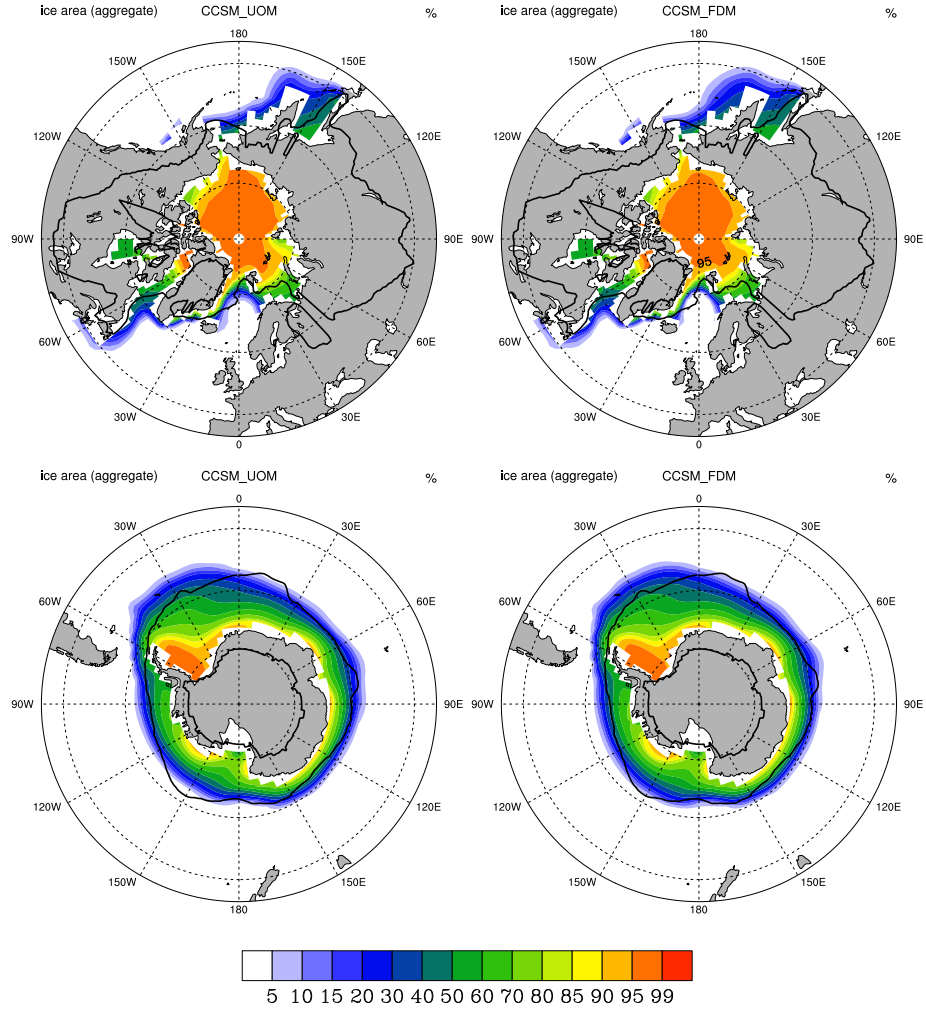
Fig. 7: Time-mean aggregated ice area for CCSM3-UOM (left) and CCSM3-FDM (right) for both hemispheres. CCSM3-FDM mean is over yr 1980-1999. Observed climatological location of 10% ice coverage from SSMI is shown by the black curve.

# RMS of SST annual mean anomaly
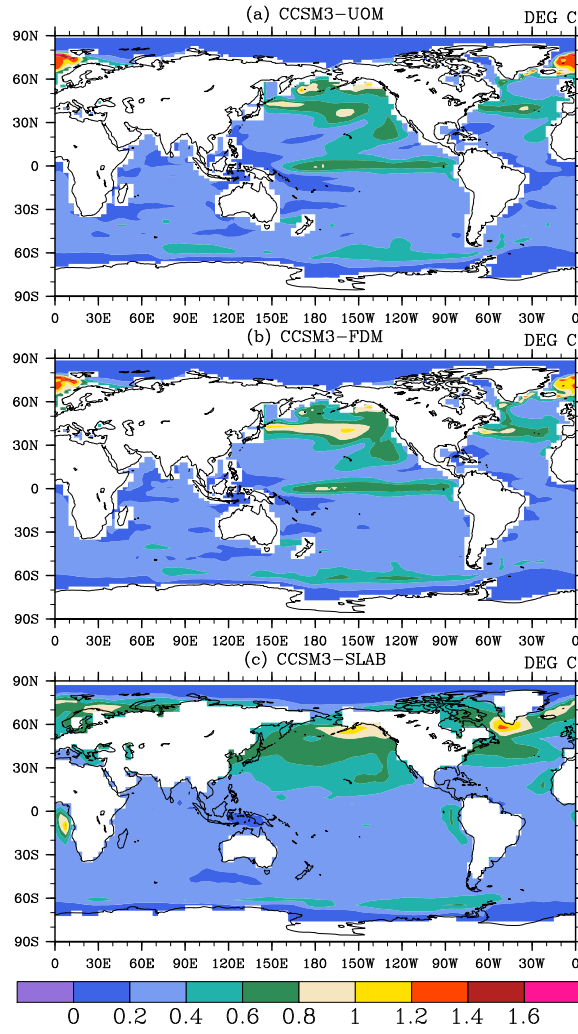


Fig. 8: Standard deviations of annual mean SST anomalies for (a) CCSM3-UOM, (b) CCSM3-FDM, and (c) CCSM3-SOM.
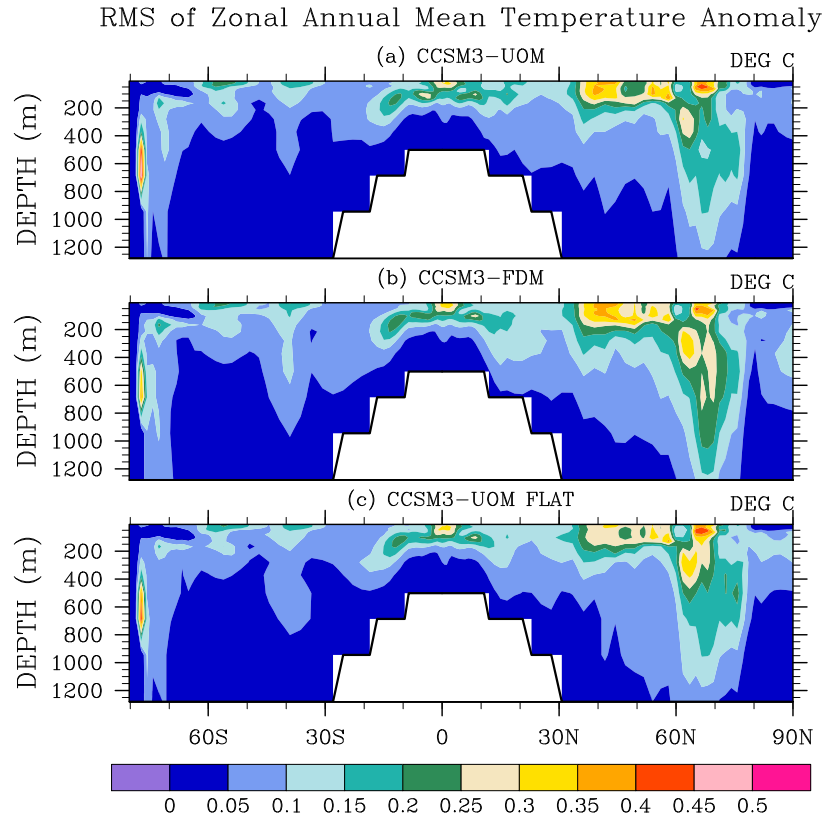
Fig. 9: Standard deviations of zonal annual mean temperature anomalies for (a) CCSM3-UOM, (b) CCSM3-FDM, and (c) CCSM3-FLAT. The bottom portion of (c) is masked out to be consisten with (a) and (b).

(a) BSF Spectrum

(b) SST Spectrum

(c) NORTH - SOUTH RHO

(d) NORTH - SOUTH BSF

(e) NORTH - SOUTH SST

(f) WSC REGRESSION
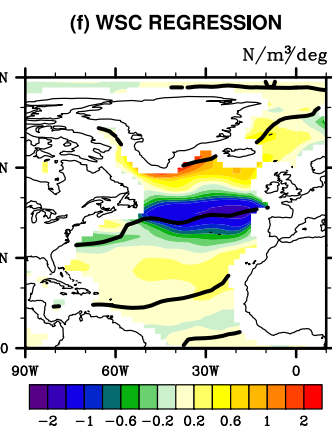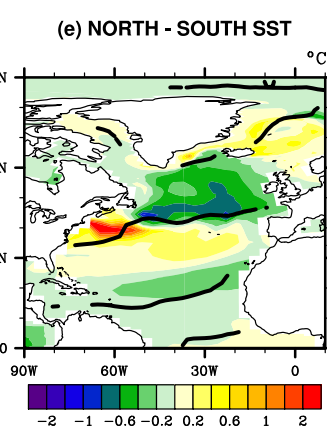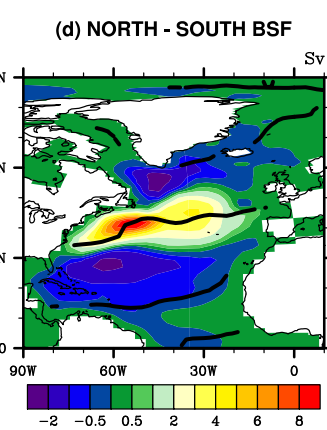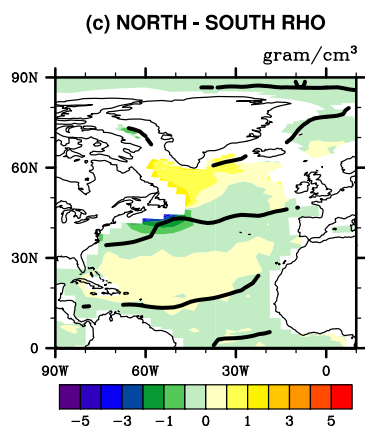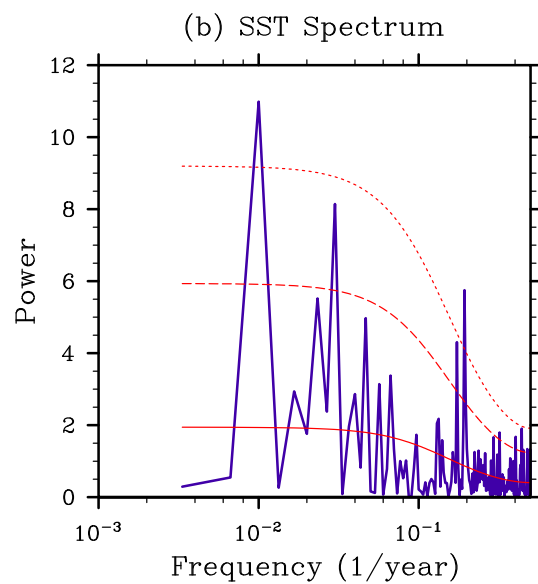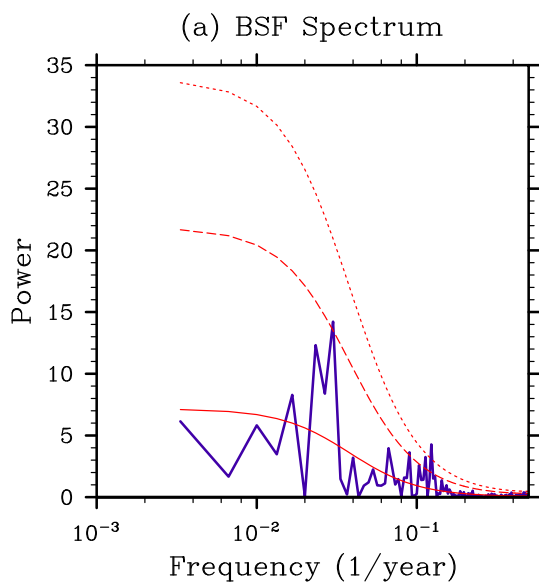
Fig. 10: CCSM3-FDM: power spectrum of the time series of (a) GBI (see text) and (b) annual mean SST anomalies at $(61°W, 41°N)$, the reference red noise spectrum with the same total variance is given by the red solid line, and the dashed and dotted lines show its 95% and 99% confident limts, respectively; NORTH-SOUTH (see text) composite for (c) potential density in the abyssal ocean, (d) BSF, and (e) SST; (f) simultaneous WSC regression with the time series of GBI. Thick solid lines show the zero isocontour of the mean WSC.

Fig. 11: Same as in Fig. 10, but for CCSM3-UOM. Note the potential density composite in (c) is for the upper ocean only.

(a) BSF Spectrum

(b) SST Spectrum

(c) NORTH - SOUTH RHO — gram/cm³

(d) NORTH - SOUTH BSF — Sv

(e) NORTH - SOUTH SST — °C
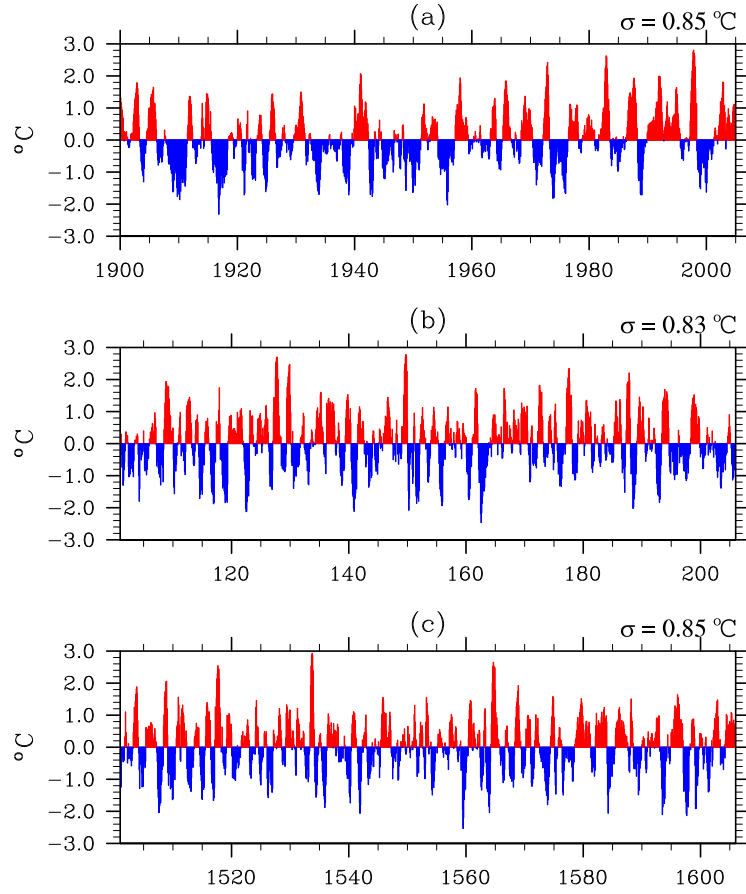
(f) WSC REGRESSION — N/m²/deg
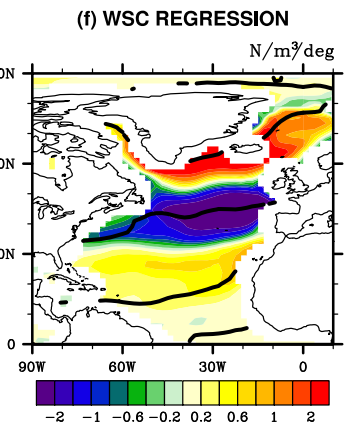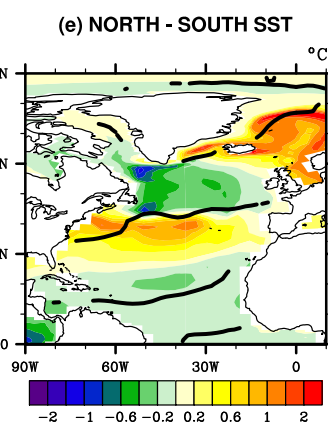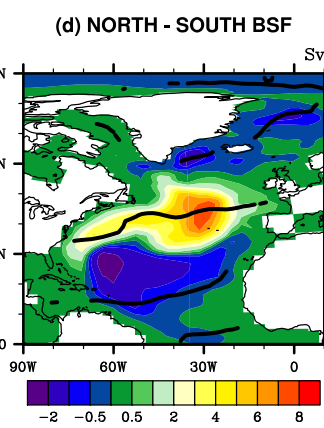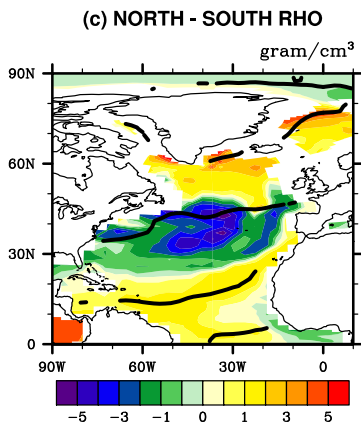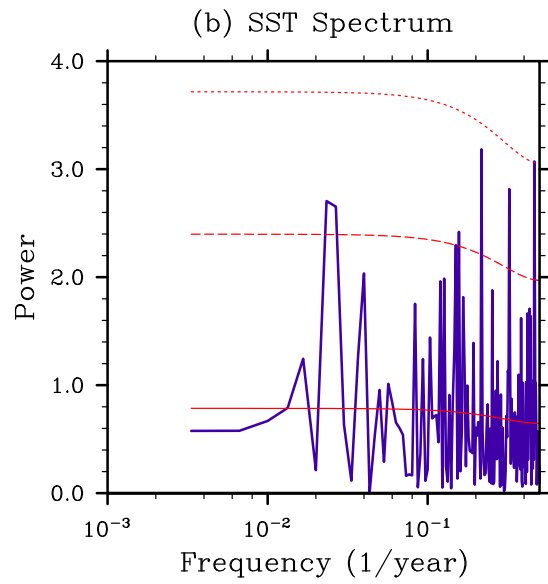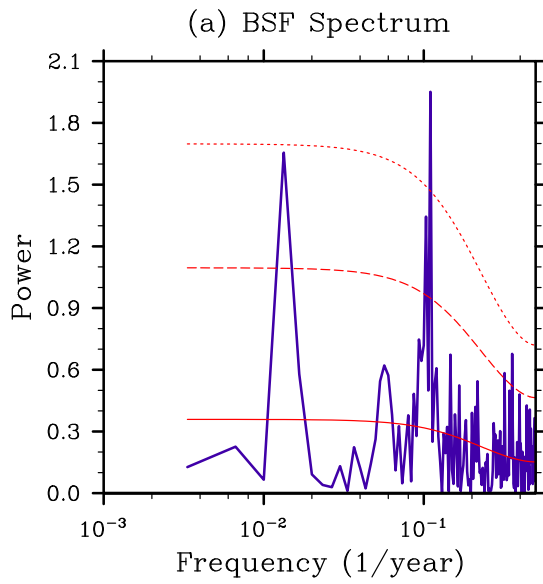
Fig. 12: Time series of monthly SST anomalies in the Niño-3.4 region. (a) observations (ERSSTv2, 1900-2004), (b) CCSM3-UOM (100-204) and (c) CCSM3-FDM (1500-1604). The standard deviations of the time series are given at the upper right of each panel, and those for models are based on the full model years analyzed.
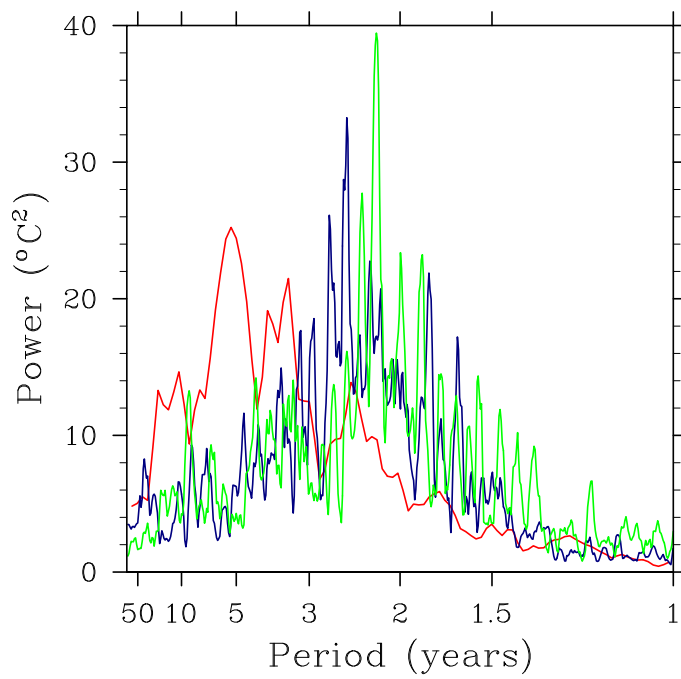
36

Fig. 13: Power spectra of the monthly Niño-3.4 SST anomalies from observations (red; ERSSTv2, 1900-2004), CCSM3-UOM (blue; model yrs 101-600) and CCSM3-FDM (green; model yrs 1501-2000).
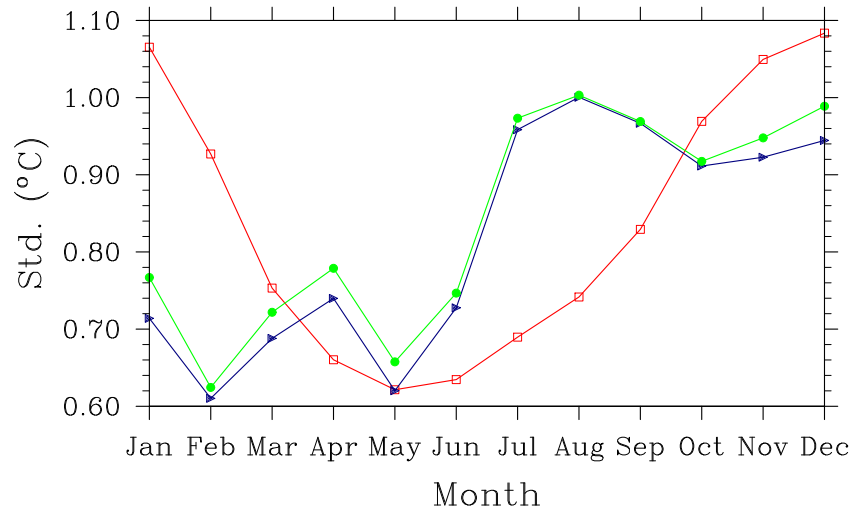
Fig. 14: Std. of monthly Niño-3.4 SST anomalies as a function of calendar months from observations (red; ERSSTv2, 1900-2004), CCSM3-UOM (blue; model yrs 101-600) and CCSM3-FDM (green; model yrs 1501-2000).

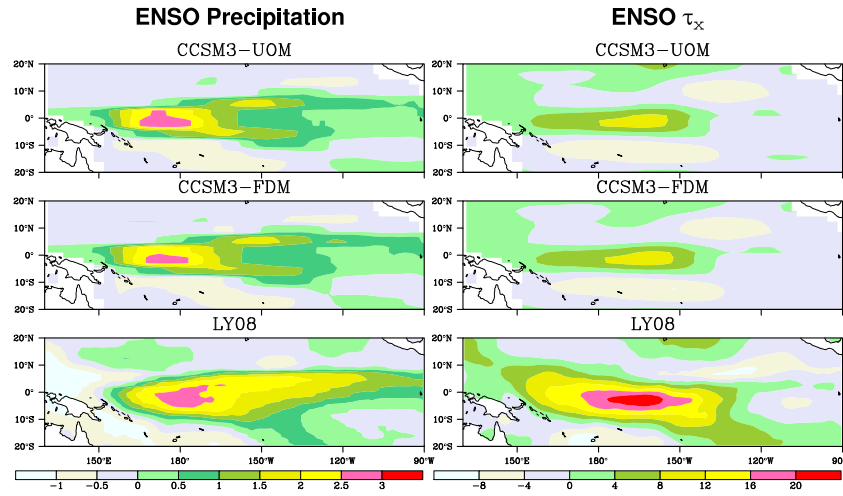**ENSO Precipitation**      **ENSO $\tau_x$**

Fig. 15: Regression of monthly (left) precipitation and (right) zonal wind stress anomalies onto Niño-3.4 SST anomalies from (top) CCSM3-UOM, (middle) CCSM3-FDM, and (bottom) observations. Observations are LY08 precipitation and stress anomalies regressed onto the ERSSTv2 over 1978-2004.
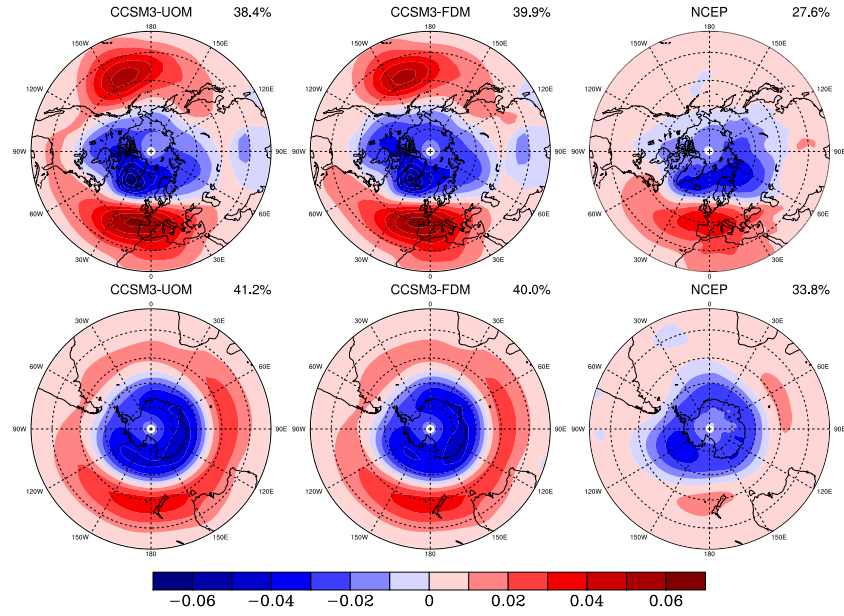
Fig. 16: (top) The first EOF of mean December-February mean sea level pressure north of $20°N$, and (bottom) the first EOF of monthly sea level pressure south of $20°S$, for CCSM3-UOM (years 101-300), CCSM3-FDM (years 1501-1700), and NCEP observations (1948-2006).
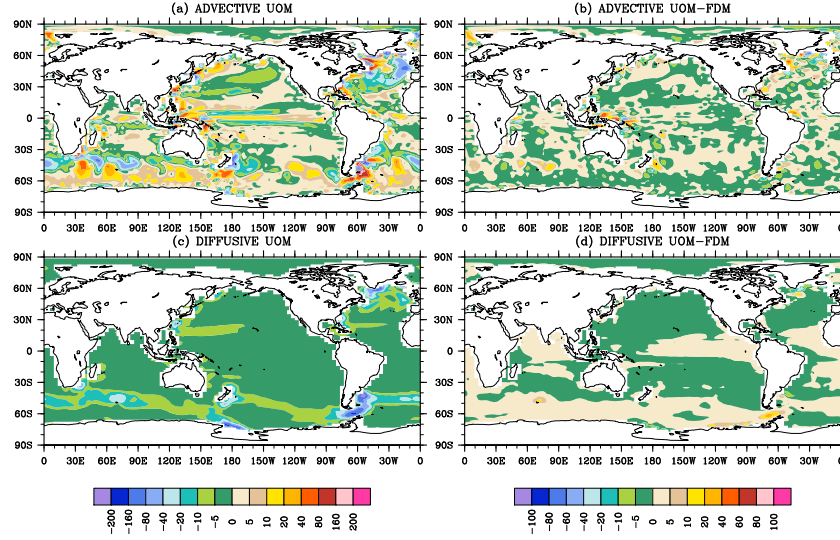
Fig. 17: Time-mean vertical advective heat flux (in $Wm^{-2}$) through the bottom of the upper ocean domain for (a) CCSM3-UOM, (b) difference between CCSM3-UOM and CCSM3-FDM; diffusive heat flux for (c) CCSM3-UOM, and (d) difference between CCSM3-UOM and CCSM3-FDM. Negative (positive) values indicate the flux is cooling (warming) the upper ocean.